Commun. Comput. Phys.
doi: 10.4208/cicp.240714.260315a

Vol. **18**, No. 5, pp. 1445-1460
November 2015

Heat Jet Approach for Atomic Simulations at Finite Temperature

Shaoqiang Tang* and Baiyili Liu

HEDPS, CAPT, and LTCS, College of Engineering, Peking University, Beijing 100871, P.R. China.

Received 24 July 2014; Accepted (in revised version) 26 March 2015

Abstract. In this paper, we propose a heat jet approach for atomic simulations at finite temperature. Thermal fluctuations are injected into an atomic subsystem from its boundaries, without modifying the governing equations for the interior domain. More precisely, we design a two way local boundary condition, and take the incoming part of a phonon representation for thermal fluctuation input. In this way, non-thermal wave propagation simulations are effectively performed at finite temperature. We further apply this approach to nonlinear chains with the Morse potential. Chains with model parameters fitted to carbon and gold are simulated at room temperature with fidelity.

PACS: 05.10.-a, 02.70.Ns

Key words: Heat jet, thermostat, atomic simulations, finite temperature.

1 Introduction

Atomic simulations, or molecular dynamics simulations, have become instrumental for materials science and engineering at nano-scale or sub-micron scale. When mechanical behaviors are considered, technical and conceptual difficulties arise and make finite temperature simulations a challenging task. As the simulated system lies away from thermal equilibrium, both theoretical understanding and numerical treatments are still under active investigations in statistical and computational physics.

In a finite temperature atomic simulation, even the definition of temperature can be sophisticated. Consider an atomic lattice shown schematically in Fig. 1. The vast surrounding region represents a heat bath at a certain target temperature. When there are purely thermal fluctuations, the lattice temperature may be calculated from the temporal/ensemble average of the kinetic energy. When non-thermal motion presents, such as

*Corresponding author. *Email addresses:* maotang@pku.edu.cn (S. Tang), lbyili@pku.edu.cn (B. Liu)

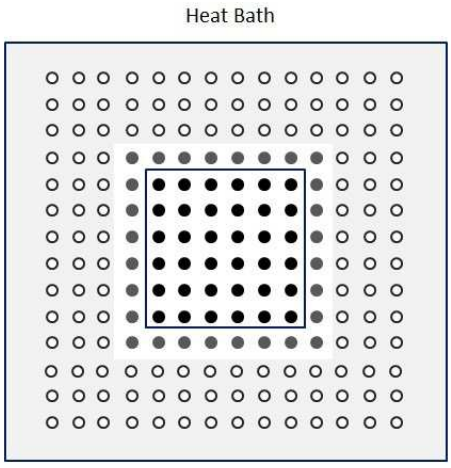

Figure 1: Schematic plot of an atomic lattice: solid dots represent atomic subsystem, gray dots represent boundary atoms, hollow circles represent surrounding atoms, and heat bath is around the outer boundary of the lattice.

in dynamical crack tip propagation, one can hardly decompose the whole motion into a crack part and a thermal part, as they both contain wave components in the full band. In a practical atomic simulation, one usually treats a small subsystem (enclosed by the interior square here) where important physics or mechanical behaviors take place, in order to reduce the numerical cost. Then the deviation between the true temperature and the calculated average kinetic energy can be big, and considerably contaminate the lattice dynamics through nonlinear interactions [1].

In this paper, we pursue a humble goal for finite temperature atomic simulations. While the exact dynamics of the subsystem should be obtained from a finite temperature simulation for the entire lattice, it may be reproduced/approximated if a suitable treatment is supplemented at its numerical boundaries. Here we aim at designing a treatment to accurately resolve non-thermal waves if the subsystem is at zero temperature; meanwhile to maintain a target temperature if there is no non-thermal motion. We assert that a finite temperature atomic simulation may be realized by this algorithm, with both the non-thermal motion and the thermal fluctuations included simultaneously.

There are extensive studies in the literature for both aspects, yet separately. The accurate resolution at zero temperature may be reached by using artificial boundary conditions in atomic simulations, or interfacial treatments for concurrent multiscale simulations [2]. We remark that several concurrent multiscale algorithms tackles with finite temperature, e.g., [3–7]. On the other hand, there are extensive studies on heat baths [8]. To name a few, one may simply rescale the velocity [9], to refresh the velocity of a randomly chosen atom [10], to add a source term together with a damping term satisfying the fluctuation-dissipation relation [11], or to add additional degrees of freedom feeding back acceleration or deceleration [12, 13]. These heat baths modify the dynamics of inte-

rior atoms in the subsystem, according to an estimation of the temperature deviation. Therefore, when a non-thermal motion presents in the subsystem, it is over-damped along with the temperature overestimation. In contrast, a phonon heat bath was proposed for linear lattices, where the thermal fluctuations are input at the boundaries [14]. Making use of a phonon representation of thermal fluctuations, this approach only modifies the force term at the boundary atoms via time history convolutions. It then allows non-thermal motions added on top of the thermal ones, and hence realizes reliable finite temperature atomic simulations, e.g., for a moving dislocation [15]. This boundary treatment involves lattice Green's functions, which have been explored in [16, 17], etc.

In this paper, we propose a heat jet approach for finite temperature atomic simulations from a wave point of view. Same as the phonon heat bath approach, we inject thermal fluctuations at the boundary atoms only, yet by a source term in a two way boundary condition that relates nearby atomic velocities and displacements. The two way boundary condition is similar to that proposed in [18], yet based on a matching boundary condition [19]. Like a wave-diode, it allows efficient transmission for thermal and non-thermal waves outward from the atomic subsystem, as well as effective injection of incoming thermal fluctuations. Meanwhile, the source term is formed with the incoming part of the phonon representation for thermal fluctuations. By avoiding the expensive time convolutions, we considerably enhance the numerical efficiency, and do not require the system to be linear. Moreover, the boundary treatment and the source term are developed separately. If any other representation of the thermal fluctuations is available, we may use it to substitute the phonon representation. This adaptiveness and the numerical efficiency provide a better chance for extending the heat jet approach to nonlinear lattices and multidimensional lattices.

In the following, we illustrate the heat jet approach for linear harmonic lattice in one space dimension in Section 2. Then in Section 3, we apply it to nonlinear lattices, and explore numerically the effective temperature range for chains with model parameters fitted to carbon and gold. Some discussions are made in Section 4.

2 Linear lattice

2.1 Formulation

We consider a linear harmonic lattice governed by the Newton equation

$$m\ddot{u}_n = k(u_{n-1} - 2u_n + u_{n+1}). \tag{2.1}$$

Here m is the mass, and k is the elastic constant. We rescale the displacement u_n by the lattice constant h_a, and time by $\sqrt{m/k}$. The non-dimensionalised equation reads

$$\ddot{u}_n = u_{n-1} - 2u_n + u_{n+1}. \tag{2.2}$$

While the entire lattice includes atoms numbered for all integers, we simulate a subsystem that contains atoms numbered from 1 to N. Following [18] and [19], we construct

a two way boundary condition based on a second order Newton-Taylor type matching boundary condition.

A monochromatic left-going wave at a wave number $\xi\in[0,\pi]$ takes the form of $u_k(t)\sim e^{i(\omega t+\xi k)}$, with a dispersion relation

$$\omega=2\sin\frac{\xi}{2}. \tag{2.3}$$

With a matching boundary condition, we relate the displacements and velocities near the boundary in a linear form.

$$\sum_{p=0}^{P}\alpha_p\dot{u}_p-\sum_{p=0}^{P}\beta_p u_p=0. \tag{2.4}$$

Substituting the wave form and discarding a common factor, we define a matching residual function

$$\Delta(\xi)=i\omega(\xi)\sum_{p=0}^{P}\alpha_p e^{i\xi p}-\sum_{p=0}^{P}\beta_p e^{i\xi p}. \tag{2.5}$$

This residual function measures the inconsistency for imposing the linear relation (2.4) on a left-going wave. For a particular choice of parameters $\{\beta_1,\cdots,\beta_P,\alpha_1,\cdots,\alpha_P\}$, transparent transmission is reached at a certain wave number if the residual function vanishes there. As long waves usually dominate the energy band, we take $P=3$ and require $\Delta(\xi)=o(\xi^2)$ and $\Delta(\pi/2)=0$. After some calculations, this amounts to

$$\dot{u}_1=-\alpha_2\dot{u}_2-\dot{u}_3+\beta_1u_1+\beta_3u_3, \tag{2.6}$$

with $\alpha_2=2+2\sqrt{2},\beta_1=-\beta_3=-(2+\sqrt{2})$.

Substituting the wave form $u_n=e^{i(\omega t+\xi n)}+R(\xi)e^{i(\omega t-\xi n)}$ into (2.6), the reflection coefficient may be found as

$$R(\xi)=-\frac{i\omega\left[e^{i\xi}+\alpha_2e^{i2\xi}+e^{i3\xi}\right]+\beta_3(e^{i\xi}-e^{i3\xi})}{i\omega\left[e^{-i\xi}+\alpha_2e^{-i2\xi}+e^{-i3\xi}\right]+\beta_3(e^{-i\xi}-e^{-i3\xi})}. \tag{2.7}$$

As seen from Fig. 2, the boundary condition well suppresses reflections, particularly effective over the wave number interval $[0,\pi/2]$. The reflection coefficient is less than 1 over the whole first Brillouin zone, indicating stability [20].

Next, we design a two way boundary condition based on this matching boundary condition. Assuming that a right-going wave is input in the form of $w_l(t)$ ($l=1,2,3$) for the l-th atom, we replace u_l by u_l-w_l in (2.6) and obtain

$$\dot{u}_1=-\alpha_2\dot{u}_2-\dot{u}_3+\beta_3(u_3-u_1)+f(t), \tag{2.8}$$

$$f(t)=\dot{w}_1+\alpha_2\dot{w}_2+\dot{w}_3-\beta_3(w_3-w_1). \tag{2.9}$$

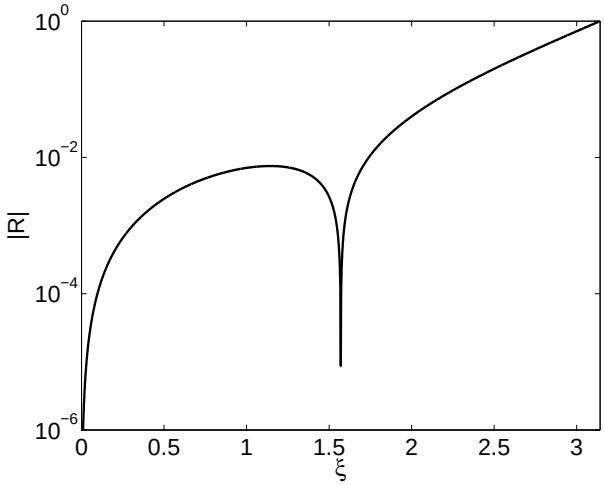

Figure 2: Reflection coefficient of matching boundary condition for harmonic lattice.

To simplify theoretical analysis, we discuss the property of a semi-infinite chain, namely, $N\to\infty$. If the initial profile is consistent with the right-going wave input, namely, $u_l(0)=w_l(0),\dot{u}_l(0)=\dot{w}_l(0)$, then the solution is $u_l(t)=w_l(t)$, reproducing the right-going wave precisely.

On the other hand, if the source term f does not cleanly represent an incoming wave, e.g., we consider a normal mode in the wrong direction, $v_l(t)\sim e^{i(\omega t+\xi l)}$ for $l=1,2,3$, and take

$$f(t)=\dot{v}_1+\alpha_2\dot{v}_2+\dot{v}_3-\beta_3(v_3-v_1). \tag{2.10}$$

Direct calculation shows that the solution to the semi-infinite chain reads

$$u_n(t)\sim\frac{i\omega\left[e^{i\xi}+\alpha_2e^{i2\xi}+e^{i3\xi}\right]+\beta_3(e^{i\xi}-e^{i3\xi})}{i\omega\left[e^{-i\xi}+\alpha_2e^{-i2\xi}+e^{-i3\xi}\right]+\beta_3(e^{-i\xi}-e^{-i3\xi})}e^{i(\omega t-\xi n)}. \tag{2.11}$$

The amplitude amplification factor is precisely $-R(\xi)$, which is small by design.

From above discussions, the two way boundary condition acts like a wave-diode, as it allows both exact injection and effective wave propagation out of the subsystem, and resists improper directional sources.

Next, we design a suitable input at the boundary. It is well known that in a harmonic chain, thermal fluctuations at temperature T take a phonon (normal mode) representation as follows [14, 21]

$$u_n(t)=\sum_p a_p^+\cos(\omega_pt+\phi_p^+)\cos\xi_pn+a_p^-\cos(\omega_pt+\phi_p^-)\sin\xi_pn. \tag{2.12}$$

Here for a chain with N atoms, $\xi_p=2\pi p/N$ is the wave number, and $\omega_p=2\sin\frac{\xi_p}{2}$ is the frequency. In the following, if not specified otherwise, we take ξ_p within the interval

$[\pi/8,7\pi/8]$ with a step size $\Delta\xi=\pi/100$. This gives $N_c=76$ normal modes, for which the amplitude follows the Gibbs distribution with [14, 21]

$$<(a_p^{\pm})^2>=\frac{2T}{N_c\omega_p^2}, \tag{2.13}$$

where the temperature is rescaled by kh_a^2/k_B, with the Boltzmann constant $k_B=1.38\times 10^{-23}$J/K.

After some manipulations, we find that the right-going wave component in (2.12) is $\tilde{a}_p\cos(\omega_p t-\xi_p n+\varphi_p)$, with

$$\tilde{a}_p^2=\frac{1}{4}\left[(a_p^+)^2+(a_p^-)^2+2a_p^+a_p^-\sin(\phi_p^+-\phi_p^-)\right], \tag{2.14}$$

$$\varphi_p=\arctan\frac{a_p^+\sin\phi_p^++a_p^-\cos\phi_p^-}{a_p^+\cos\phi_p^+-a_p^-\sin\phi_p^-}. \tag{2.15}$$

As the phases $\phi_p^{\pm}$ lie randomly between $[0,2\pi]$, it holds that φ_p is a random phase in the same interval, and

$$<\tilde{a}_p^2>=\frac{T}{N_c\omega_p^2}. \tag{2.16}$$

In the simulations, we simply take the normalized amplitude $\tilde{a}_p=\sqrt{T/N_c\omega_p^2}$.

The right boundary is treated in the same manner. If the target boundary temperatures are T_L and T_R, we summarize the complete governing system as follows

$$\ddot{u}_n=u_{n-1}-2u_n+u_{n+1},\quad n=2,\cdots,N-1, \tag{2.17}$$

$$\dot{u}_1=-\alpha_1\dot{u}_2-\dot{u}_3+\beta_3(u_3-u_1)+f^L, \tag{2.18}$$

$$\dot{u}_N=-\alpha_1\dot{u}_{N-1}-\dot{u}_{N-2}+\beta_3(u_{N-2}-u_N)+f^R, \tag{2.19}$$

$$f^L=\dot{w}_1+\alpha_1\dot{w}_2+\dot{w}_3-\beta_3(w_3-w_1), \tag{2.20}$$

$$f^R=\dot{v}_N+\alpha_1\dot{v}_{N-1}+\dot{v}_{N-2}-\beta_3(v_{N-2}-v_N), \tag{2.21}$$

$$w_l=\sum_p\sqrt{\frac{T_L}{N_c\omega_p^2}}\cos(\omega_p t-\xi_p l+\varphi_p^L), \tag{2.22}$$

$$v_l=\sum_p\sqrt{\frac{T_R}{N_c\omega_p^2}}\cos(\omega_p t+\xi_p l+\varphi_p^R). \tag{2.23}$$

2.2 Numerical tests

We simulate a subsystem with $N=200$ atoms by the second order Runge-Kutta method at a time step $\Delta t=0.01$.

First, we perform a benchmark test for the heating process. Setting all atoms at equilibrium initially, we inject heat jets at temperature $T_L=T_R=3$. As depicted in subplot (a) of

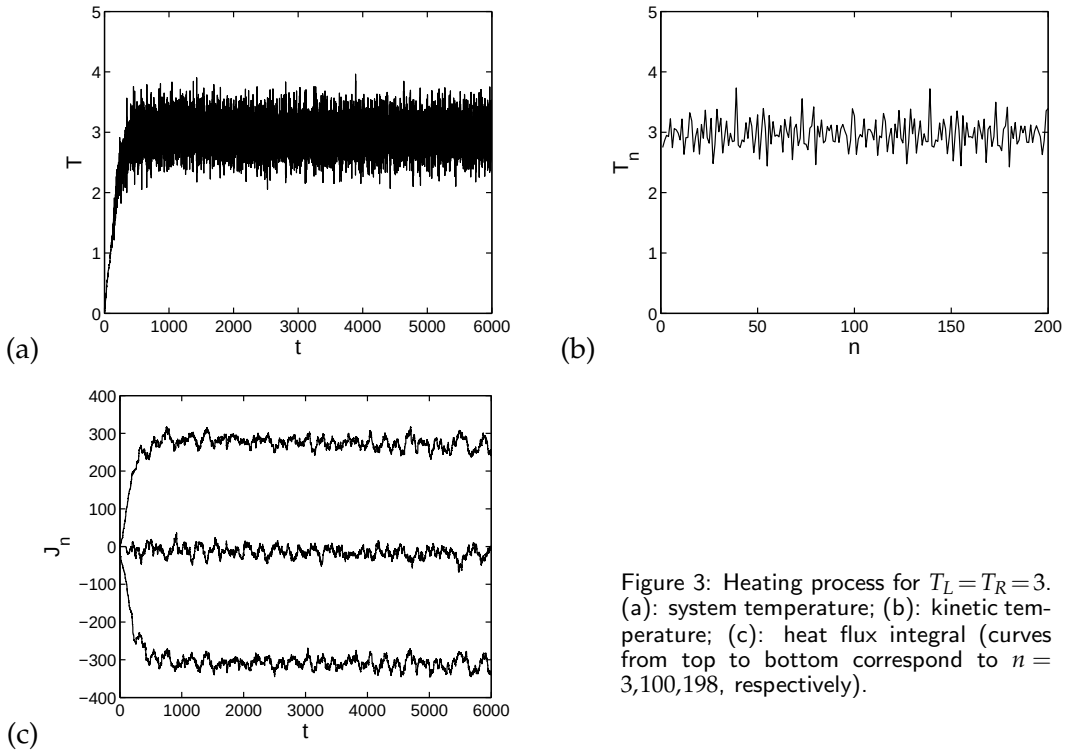

Figure 3: Heating process for $T_L = T_R = 3$. (a): system temperature; (b): kinetic temperature; (c): heat flux integral (curves from top to bottom correspond to $n =$ 3,100,198, respectively).

Fig. 3, the system temperature $T(t) = \frac{1}{N}\sum_{n=1}^{N} \dot{u}_n^2(t)$ rises up to the equilibrium temperature $T = 3$ at a time slightly after $t = 200$. This delay time comes from wave propagation across the subsystem. In subplot (b), the kinetic temperature for each atom $T_n = \frac{1}{5000}\int_{1000}^{6000} \dot{u}_n^2(t)\mathrm{d}t$ takes a random appearance. Furthermore, we display in subplot (c) the heat flux integral $J_n(t) = \int_0^t \dot{u}_{n+1}(u_n - u_{n+1})\mathrm{d}t$ at n=3,100,198, respectively. At around t=200, $J_3(t)$ increases to about 300, indicating a net energy flow toward the subsystem. It then oscillates around this level, due to thermal fluctuations. The same heat jet injection process is observed for $J_{198}(t)$, with a reverse sign. For $J_{100}(t)$, it is zero before $t = 100$, when the heat jets from both sides have not reached the center of the subsystem. It then oscillates around 0, reflecting the dynamical balance between the two reverse directional heat jets.

Next, we simulate with different temperatures for the two sides, namely, $T_L = 5$ and $T_R = 1$. In Fig. 4, the subsystem is heated to the mean temperature $T = 3$. The heating process and the kinetic temperature are similar to the previous case. However, in subplot (c), we observe that the heat jet from the right takes a smaller flux than that from the left. The net flux difference results in a slope for J_n, showing that the wave components to maintain $T = 3$ differ from the previous case. Moreover, as seen from subplot (b), there is no Kapitza effect when a thermal gradient is applied on the two ends. This demonstrates a perfect impedance match in the heat jet approach.

The range of wave number band and step size for the phonon representation affects

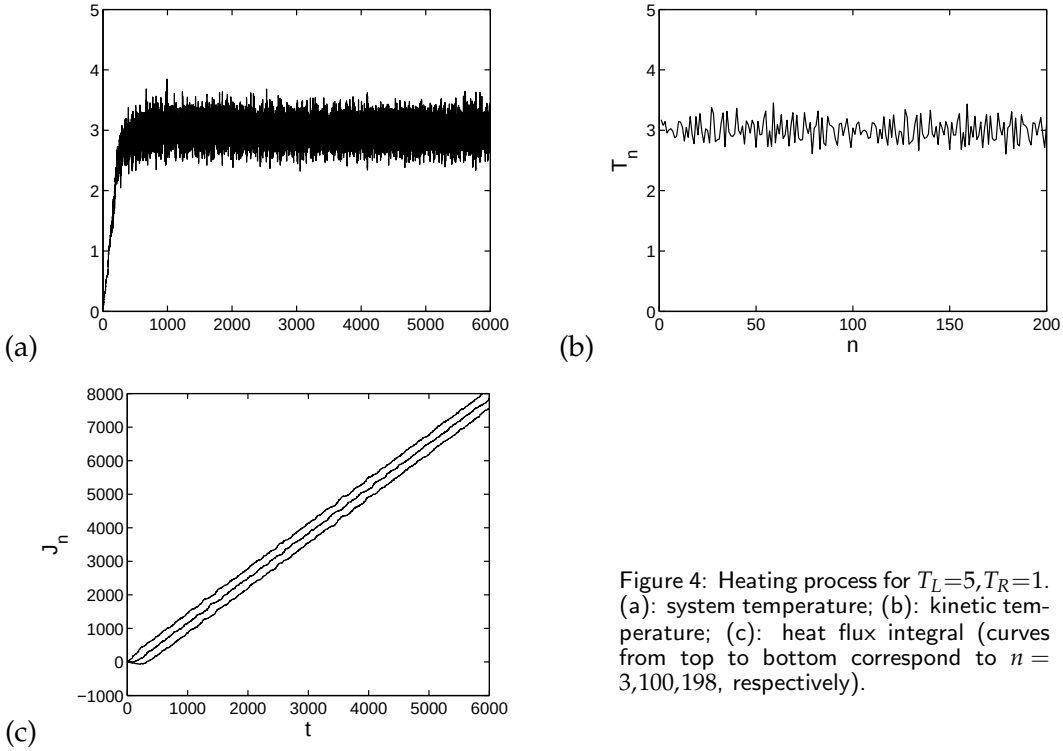

Figure 4: Heating process for T_L=5,T_R=1. (a): system temperature; (b): kinetic temperature; (c): heat flux integral (curves from top to bottom correspond to $n=$ 3,100,198, respectively).

the fluctuations in both the system temperature and the averaged kinetic temperature profile. As observed from Fig. 5 and Fig. 6, a wider range of wave number band and more modes result in smaller fluctuations. This holds for the phonon representation (2.12), which can be shown rigorously. The proposed heat jet approach faithfully reproduces this representation, hence maintains the same feature.

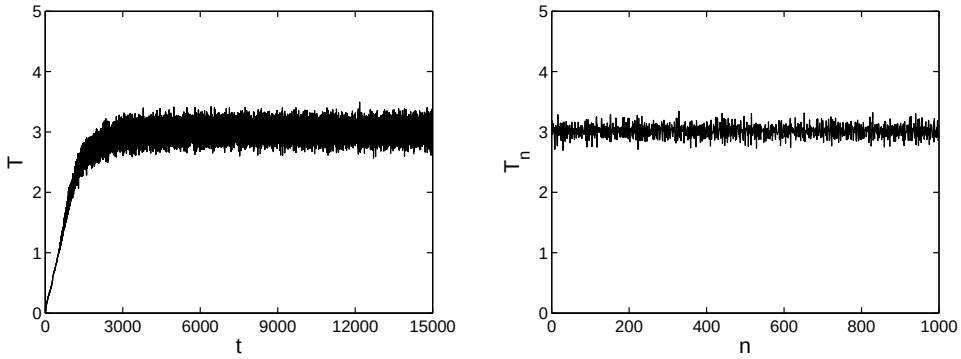

Figure 5: Heating process for $T_L = T_R = 3$ with 376 modes ($\Delta\xi = \pi/500$). Left: system temperature; right: kinetic temperature.

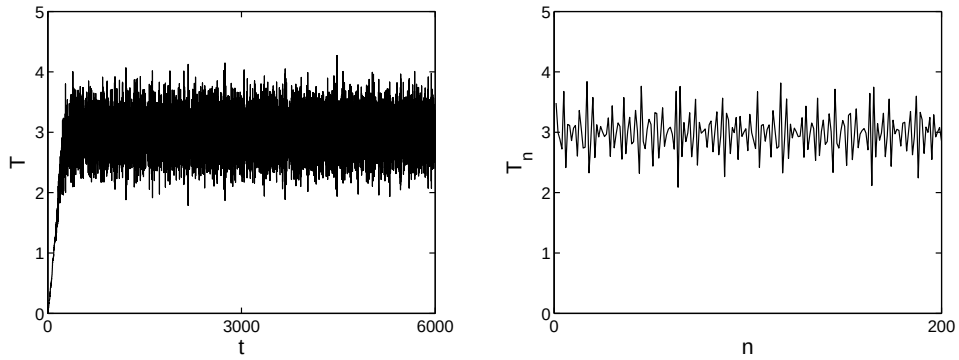

Figure 6: Heating process for $T_L = T_R = 3$ with different range of wave numbers (ξ sampled in $[\pi/4, 3\pi/4]$ with $\Delta\xi = \pi/100$). Left: system temperature; right: kinetic temperature.

Finally, we illustrate a finite temperature simulation with non-thermal motion. We first heat the subsystem to $T = 3$. At $t = 2000$, an additional motion is supplied on top of the thermal fluctuations in the form of a Gaussian hump $\tilde{u}_n = 50e^{-0.005(n-100)^2}$. We observe from Fig. 7 that this motion is fairly strong initially. It splits into two humps, propagating outward with an amplitude about half of the initial profile. At $t = 2100$, the humps reach the boundaries and vanish without observable reflection. Eventually the subsystem equilibrates at $T = 3$. See Fig. 8. The nominal system temperature during the propagation of the Gaussian hump deviates from the true system temperature $T = 3$. It is during this period that over estimation of temperature and over damping of non-thermal

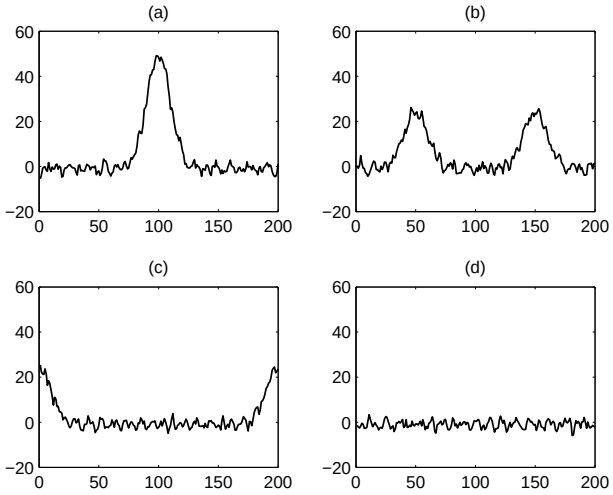

Figure 7: Finite temperature simulation of harmonic lattice: (a) $u_n(2000)$; (b) $u_n(2050)$; (c) $u_n(2100)$; (d) $u_n(2150)$.

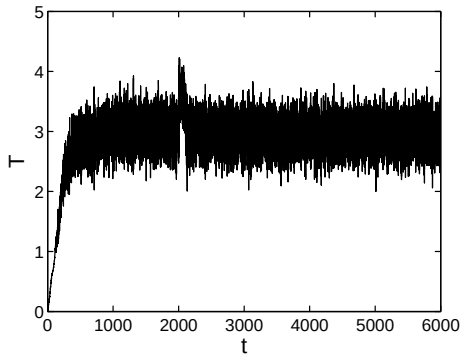

Figure 8: Nominal system temperature in finite temperature simulation of harmonic lattice.

motion likely occur, if one adopts standard heat baths such as those proposed by Nosé and Hoover, Anderson, or Berendsen [9, 10, 12, 13].

The numerical results demonstrate that the proposed heat jet approach fulfills the design goal. It allows non-thermal motion and thermal fluctuations to propagate freely out of the subsystem, while heat jets at both ends are injected into the subsystem effectively to maintain the prescribed temperature. As a matter of fact, the heat jet approach uses a linear boundary condition, and superposition holds. The linear nature makes it straightforward to support simultaneously non-thermal motion and thermal fluctuations.

3 Nonlinear lattice with Morse potential

For a nonlinear lattice, we perform a linearization and modify the two way boundary condition by the sound speed c as a factor.

$$\dot{u}_1 = -\alpha_1 \dot{u}_2 - \dot{u}_3 + c\cdot\beta_3(u_3-u_1)+f(t), \tag{3.1}$$

$$f(t) = \dot{w}_1 + \alpha_1 \dot{w}_2 + \dot{w}_3 - c\cdot\beta_3(w_3-w_1). \tag{3.2}$$

To illustrate the heat jet approach for a nonlinear lattice, we consider the Morse potential with nearest neighboring interaction

$$V_M(r) = \varepsilon\left(e^{-2\alpha(r-r_0)} - 2e^{-\alpha(r-r_0)}\right). \tag{3.3}$$

We rescale the displacement by $1/\alpha$, time by $\sqrt{m/2\varepsilon}/\alpha$, and mass by m. Accordingly, temperature is rescaled by $2\varepsilon/k_B$.

If we fit for carbon, the parameters are $r_0 = 1.39\times10^{-10}$m, $\alpha = 2.625\times10^{10}\text{m}^{-1}$, $\varepsilon = 6.03105\times10^{-19}$J. Moreover, the mass of a carbon atom is $m = 1.993\times10^{-26}$kg [22]. Temperature is then rescaled by 8.7407×10^{4}K, and time by 4.8968fs.

Under these scalings, the Newton equation reads

$$\ddot{u}_n = -e^{-2(u_{n+1}-u_n)} + e^{-(u_{n+1}-u_n)} + e^{-2(u_n-u_{n-1})} - e^{-(u_n-u_{n-1})}. \tag{3.4}$$

Performing Taylor expansion for the righthand side, we find the first two terms as

$$(u_{n-1}-2u_n+u_{n+1})\left[1-\frac{3}{2}(u_{n+1}-u_{n-1})\right]. \tag{3.5}$$

Hence, we take the sound speed $c=1$, and the atomic strain $(u_{n+1}-u_{n-1})$ indicates the nonlinearity strength. A rough estimation shows that $(u_{n+1}-u_{n-1})$ is proportional to $\sqrt{T}$. In Fig. 9, the system temperature equilibrates quickly toward a temperature slightly lower than the target temperature. As a matter of fact, the heat jet approach produces

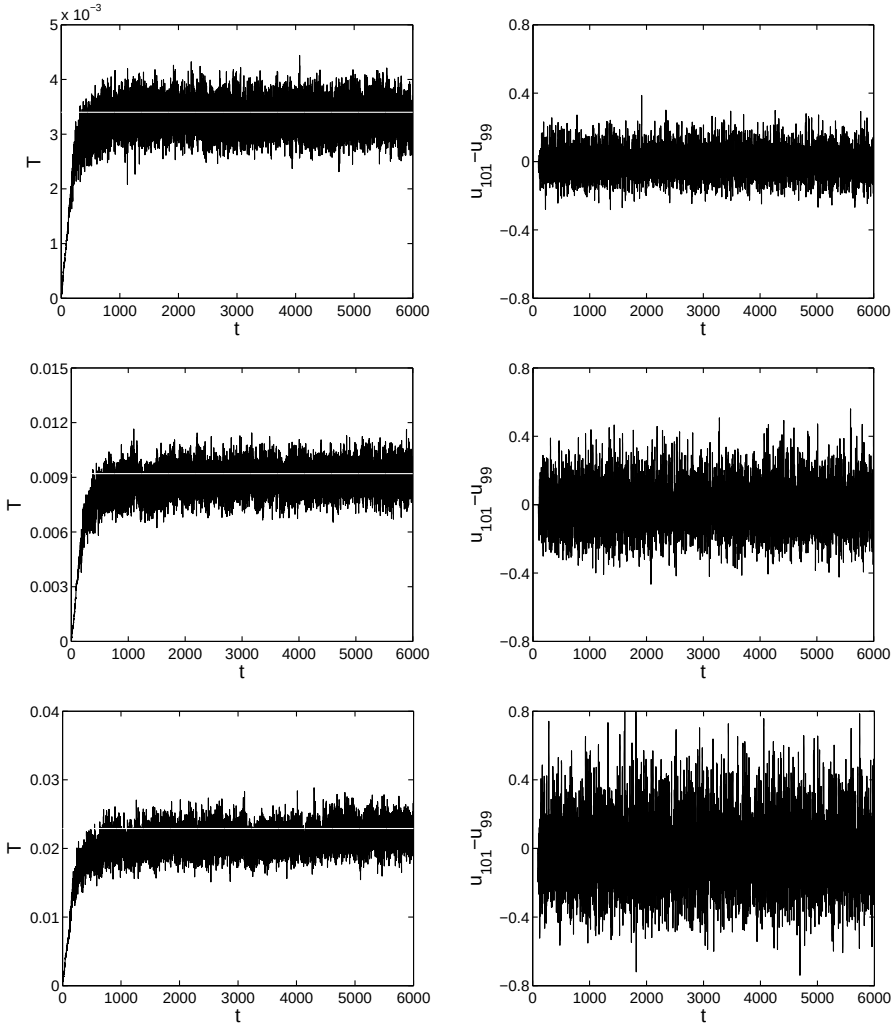

Figure 9: System temperature and corresponding atomic strain $(u_{101}(t)-u_{99}(t))$ for nonlinear lattice with the Morse potential where the parameters are fitted to carbon (horizontal level line represents the target temperature). Top: $T_L=T_R=0.0034$ (300K); middle:$T_L=T_R=0.0092$ (800K); bottom: $T_L=T_R=0.0229$ (2000K).

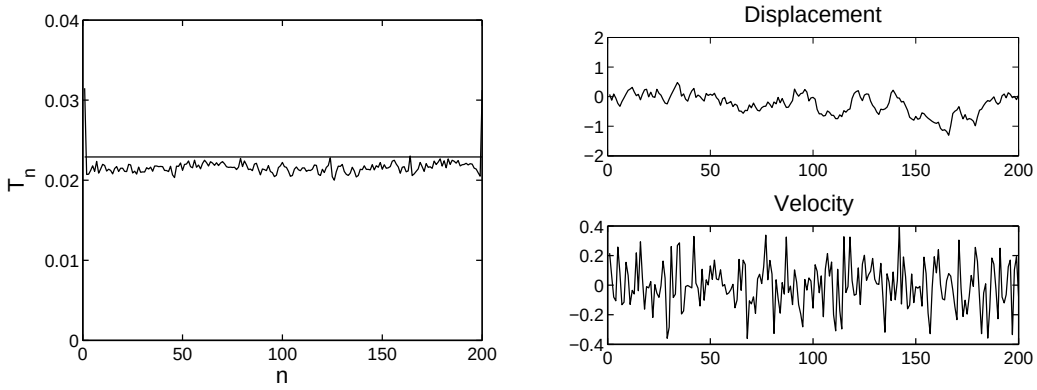

Figure 10: Nonlinear lattice with the Morse potential where the parameters are fitted to carbon at target temperature $T_L = T_R = 0.0229$ (2000K). Left: kinetic temperature (horizontal level line represents the target temperature); upper-right: displacement snapshot; lower-right: velocity snapshot.

satisfactory results at room temperature 300K ($T_L = T_R = 0.0034$). At 800K, the resulting system temperature is roughly 3% lower. At 2000K, the system temperature deviates for only about 5%. Corresponding to the deviations, the subplots for $(u_{101} - u_{99})$ in the right column show that the nonlinearity increases along with the target temperature.

There are two major relevant factors attributing to this deviation. First, the thermal fluctuation input at the boundary atoms does not fit when nonlinearity becomes strong, because the phonon representation is exact only for the linear harmonic lattice. Secondly, the effective reflection suppression by the boundary condition needs to be reconsidered. The first one may lead to a lower temperature, whereas the second one may trap more kinetic energy inside the atomic subsystem. The resulting lower system temperature indicates that the first factor dominates in this case. A more direct clue is the left subplot in Fig. 10. While the first atom takes a bigger kinetic energy, there appears a boundary layer right next to it, and the kinetic temperature drops below the target temperature for all interior atoms.

With the heat jet approach validated for this nonlinear lattice, we perform a finite temperature simulation at 300K with an additional motion again at $t = 2000$, when the lattice is at thermal equilibrium. The additional motion takes the form of $\tilde{u}_n = 1.5e^{-0.005(n-100)^2}$. The big amplitude here is close to that induced by a dislocation. The numerical results in Fig. 11 and Fig. 12 show effectiveness similar to that in the harmonic lattice simulation.

We note that nonlinearity depends on the type of atom and the potential. For instance, if fitted to gold, one takes $r_0 = 2.922 \times 10^{-10}$m, $\alpha = 1.637 \times 10^{10}\text{m}^{-1}$, $\varepsilon = 8.9712 \times 10^{-20}$J, and $m = 3.2708 \times 10^{-25}$kg [14]. Accordingly, the temperature is rescaled by 1.3002×10^4K, and time by 82.4780fs. For room temperature 300K, the corresponding rescaled temperature is $T = 0.0231$, which is about that for carbon at 2000K. The system temperature in Fig. 13 is comparable to that in the bottom row of Fig. 9. This verifies that it is nonlinearity that influences the fidelity of the heat jet approach.

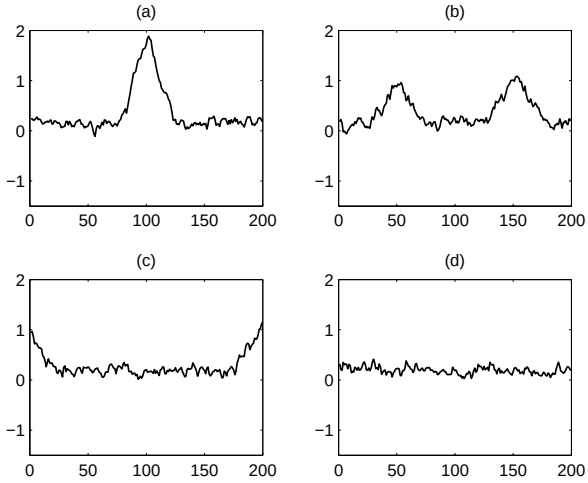

Figure 11: Finite temperature simulation of nonlinear lattice with the Morse potential where the parameters are fitted to carbon: (a) $u_n(2000)$; (b) $u_n(2050)$; (c) $u_n(2100)$; (d) $u_n(2150)$.

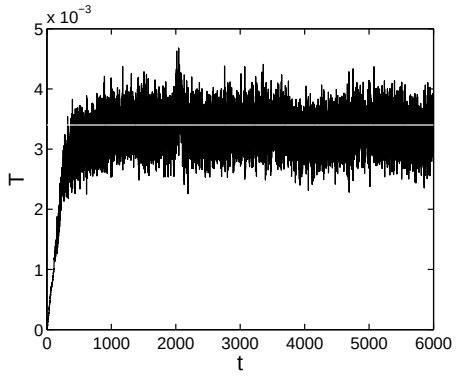

Figure 12: Nominal system temperature in finite temperature simulation of nonlinear lattice with the Morse potential where the parameters are fitted to carbon (horizontal level line represents the target temperature).

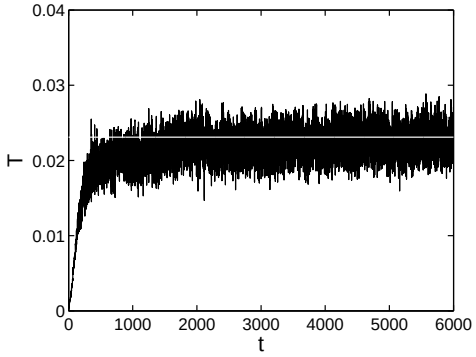

Figure 13: System temperature for a chain with Morse potential where the parameters are fitted to gold at target temperature $T_L = T_R = 0.0231$ (300K) (horizontal level line represents the target temperature).

4 Discussions

From the wave viewpoint, we have proposed a heat jet approach for finite temperature atomic simulations with fidelity. We note that the wave viewpoint have also been adopted by other researchers in different contexts, e.g., [21, 23]. The fidelity originates from an accurate boundary treatment. It filters waves according to their propagation directions, hence serves like a wave diode. In case of a linear lattice, the error is rigorously bounded by the reflection coefficient, which is small by design. If more boundary atoms are used in the treatment, we may further improve the fidelity, as seen from the reflection coefficient analysis in [19]. Furthermore, we adopt the incoming components of a phonon (normal mode) representation for the thermal fluctuation input. In this way, we avoid the error caused by injecting wrong directional waves into the subsystem. Although in nonlinear lattices, the wrong directional waves may seemingly help reaching the target temperature, the phonon distribution is further distorted, as the more-likely reflected modes have a better chance to be injected in. We remark that the displacement in a stand-alone lattice with the standard Nose-Hoover heat bath may not be adopted for thermal fluctuation input. The problem comes from a time rescaling in this heat bath, which makes the displacement not representing the correct dynamics of a harmonic lattice, even though the statistic properties and the phase space behaviors are correct.

There are various ways in treating lattices with stronger nonlinearity. Because a correct input turns out to be the bottle-neck, and such correct input is not available at this moment for a system away from thermal equilibrium, we suggest to construct the input by taking the displacement of a stand-alone lattice with the heat jet injected at its boundary, and rescale the amplitudes in the Berendsen way [9]. Then this rescaled input is effectively injected into the subsystem for finite temperature simulations.

For a lattice in multiple dimensions, we note that the heat jet approach works equally well, provided that the boundary treatment is effective, and the thermal fluctuation input is accurate. For the former, the matching boundary condition has been shown effective in reflection suppression for various lattice structures [19, 24]. Two way boundary conditions may be constructed then according to [18]. For the latter, we notice that the normal mode representation still works. As there are many incoming modes, the summing up of all modes may induce heavy numerical cost and a more effective algorithm is demanded.

Due to its linear nature, the heat jet approach applies readily to multiscale simulations. One important issue is the displacement drift, which represents a translation of the whole atomic subsystem. For instance, see the middle subplot of Fig. 10, and subplot (d) of Fig. 11. In a pure atomic simulation, the drift does not matter much for the dynamics, as only velocity profile influences the temperature. However, in a multiscale simulation, spurious translation may be passed to the coarse scale region and change dynamics there. A rigorous derivation shows that we need to put a constraint on initial velocity profile for the subsystem, as well as a treatment on initial thermal fluctuation for the boundary atoms. In this way, we may avoid displacement drift and reproduce the correct dynamics. Under the framework of a finite difference multiscale approach [25],

we have successfully performed such multiscale simulations for linear harmonic lattice. It will be reported in a forthcoming publication.

Acknowledgments

This research is partially supported by NSFC under contract number 11272009. We would also like to thank Mr. Xin Wang at Georgia Institute of Technology, and Mr. Shengkai Wang at Stanford University for their stimulating discussions in an earlier stage for developing the heat jet approach.

References

[1] H. Jiang, Y. Huang and K.C. Hwang, A finite-temperature continuum theory based on interatomic potentials, Trans. ASME, 127(2005), 408-416.
[2] W.K. Liu, E.G. Karpov and H.S. Park, Nano Mechanics and Materials: Theory, Multi-Scale Methods and Applications. Wiley: New York, 2006.
[3] L. Dupuy, E.B. Tadmor, R.E. Miller and R. Phillips, Finite temperature quasicontinuum: molecular dynamics without all the atoms, Phys. Rev. Lett., 95(2005), 060202.
[4] X. Li and W. E, Multiscale modeling of the dynamics of solids at finite temperature, J. Mech. Phys. Solids, 53(2005),1650-1685.
[5] X. Liu and S. Li, Nonequilibrium multiscale computational model, J. Chem. Phys., 126(2007), 124105.
[6] N. Mathew, R.C. Picu and M. Bloomfield, Concurrent coupling of atomistic and continuum models at finite temperature. Comput, Methods Appl. Mech. Engrg., 200(2011), 765-773.
[7] M.Z. Xiang, J.Z. Cui, B.W. Li and X. Tian, Atomic-continuum coupled model for thermomechanical behavior of materials in micro-nano scales, Sci. China-Phys. Mech. Astron., 55(2012), 1125-1137.
[8] S. Lepri, R. Livi and A. Politi, Thermal conduction in classical low-dimensional lattices. Physics Reports, 377(2003), 1-80.
[9] H.J.C. Berendsen, J.P.M. Postma, W.F. van Gunsteren, A. DiHola and J.R. Haak, Molecular dynamics with coupling to an external bath, J. Chem. Phys., 81(1984), 3684-3690.
[10] H.C. Anderson, Molecular dynamics simulation at constant pressure and/or temperature, J. Chem. Phys., 72(1980), 2384-2393.
[11] G. Bussi and M. Parrinello, Accurate sampling using Langevin dynamics, Phys. Rev. E., 75(2007), 056707.
[12] W.G. Hoover, Canonical dynamics: equilibrium phase-space distributions, Phys. Rev. A., 31(1985), 1695-1697.
[13] S. Nosé, A unified formulation of the constant temperature molecular dynamics methods, J. Chem. Phys., 81(1984), 511-519.
[14] E.G. Karpov, H.S. Park and W.K. Liu, A phonon heat bath approach for the atomistic and multiscale simulation of solids, Int. J. Numer. Meth. Eng., 70(2007), 351-378.
[15] S. Tang, W.K. Liu, E. Karpov and T.Y. Hou, Bridging atomistic/continuum scales in solids with moving dislocations, Chin. Phys. Lett., 24(2007), 161-164.

[16] E.G. Karpov, G.J. Wagner and W.K. Liu, A Green's function approach to deriving non-reflecting boundary conditions in molecular dynamics simulations, Int. J. Numer. Methods Engrg., 62(2005), 1250-1262.
[17] D.E. Farrell, E.G. Karpov and W.K. Liu, Algorithms for bridging scale method parameters, Comput. Mech., 40(2007), 965-978.
[18] S. Tang, A two-way interfacial condition for lattice simulations, Adv. Appl. Math. Mech., 2(2010), 45-55.
[19] X. Wang and S. Tang, Matching boundary conditions for lattice dynamics, Int. J. Numer. Methods Eng., 93(2013), 1255-1285.
[20] S. Tang and S. Ji, Stability of atomic simulations with matching boundary conditions, Adv. Appl. Math. Mech., 6(2014), 539-551.
[21] M. Born and K Huang, Dynamical Theory of Crystal Lattices, Clarendon: Oxford, 1954.
[22] T. Belytschko, S.P. Xiao, G.C. Schatz and R.S. Ruoff, Atomistic simulations of nanotube fracture, Phys. Rev. B., 65(2002), 235430.
[23] Q.H. Tang and T.C. Wang, Lattice wave theory of molecular dynamics, Sci. China-Phys. Mech. Astron., 41(2011), 214-220.
[24] M. Fang, S. Tang, Z. Li and X. Wang, Artificial boundary conditions for atomic simulations of Face-Centered-Cubic lattice, Comput. Mech., 50(2012), 645-655.
[25] S. Tang, A finite difference approach with velocity interfacial conditions for multiscale computations of crystalline solids, J. Comput. Phys., 227(2008), 4038-4062.